Characterization of near-field holography grating masks for optoelectronics fabricated by electron beam lithography

D. M. Tennant, T. L. Koch, P. P. Mulgrew, and R. P. Gnall
AT&T Bell Laboratories, Holmdel, New Jersey 07733

F. Ostermeyer
AT&T Laboratories, Murray Hill, New Jersey 07974

J-M. Verdiell
AT&T Holmdel, New Jersey 07733

(Received 30 June 1992; accepted 24 August 1992)

Direct write e-beam lithography and reactive ion etching was used to fabricate square-wave gratings in quartz substrates which serve as pure phase masks in the near-field holographic printing of gratings. This method of fabricating these masks extends the flexibility of the printing technique by allowing both abrupt phase shifts as well as multiple grating pitches to be simultaneously printed from a single contact mask. Grating masks with periods in the 235–250 nm range have been produced and measured to be within 0.15 nm of the design period. Transmitted and diffracted beam powers have also been measured for various duty cycles and etch depths and are shown to be important parameters for "balancing" these interfering beams. Simple scalar diffraction modeling is used to qualitatively examine the dependence of diffraction on grating parameters, but the need for a more comprehensive modeling is illustrated. Prototype masks have been used to produce grating patterns on InP substrates using two different ultraviolet illumination sources: an argon ion laser and a conventional mercury lamp.

I. INTRODUCTION

Corrugated-waveguide gratings are key elements for many of the optical devices such as filters and distributed feedback (DFB) or distributed Bragg reflector (DBR) lasers that are expected to play a key role in advanced lightwave communications systems. Direct holographic exposure of resists using two interfering ultraviolet (UV) laser beams is the commonly used technique to produce the submicron-pitch gratings required in semiconductor optical devices. This method readily produces large area gratings, but is limited in the variety of devices which can be printed in a single step. Okai *et al.*[1] showed that a replica of a triangular grating made with a precision ruling machine can be used in a self-interfering mode when illuminated with a laser to print gratings in resist. This technique can be considered a form of near-field holography and was found to produce high contrast images and improved reproducibility in the printing process when the mask was properly processed to achieve a specific combination of amplitude and phase characteristics. One advantage of this process is the ability to incorporate pitch changes and therefore phase shifts within the grating in a single print.

We have used direct write e-beam lithography (EBL) and reactive ion etching (RIE) to fabricate square-wave gratings in quartz substrates which serve as pure phase masks in the near-field holographic printing of gratings. By using EBL, the flexibility of the printing technique is expanded by allowing both abrupt phase shifts as well as multiple grating pitches to be arbitrarily located on such a mask and therefore to be simultaneously printed from a single contact mask. While similar structures have been demonstrated using direct-write-on-wafer[2,3] the parallel printing technique proposed here avoids the slow serial writing process.

The principle of the printing technique is illustrated in Fig. 1. UV light is incident on the grating at an angle θ from the normal. The beam is partially transmitted (zero order) and partially diffracted (first order). These two beams then function just as in the conventional two-beam interference method mentioned above, causing a periodic intensity variation below the mask at the spatial period of the grating. This intensity pattern is used to expose photoresist that subsequently is developed and used as an etch mask for wet chemical or dry etching of the corrugated grating in the semiconductor. For large area gratings and a highly coherent illuminator, this method should in principle result in perfect interference even in the far field. For smaller area gratings, or those with nonperiodic features, or when coherence of the illuminator is lower, the necessity for near-field printing is increased.

The example in Fig. 1 includes an abrupt half-period phase shift as might be found in a $\lambda/4$-shifted DFB laser. Figure 2 illustrates an approximate modeling of the interference pattern in the intensity of the transmitted and diffracted beams as they propagate away from the mask surface. The particular case chosen here has a 240 nm-pitch grating with a half-period shift, illuminated by 364 nm highly coherent light. The example assumes that the grating has been properly fabricated to produce equal transmitted and first-order diffracted beams, and the fields are approximated after the mask by numerically evaluating the Fresnel integrals in the Fresnel diffraction approximation. Since the transmitted beam is not affected by the phase shift, the phase-shift location in the interference pattern generally follows the propagation direction of the dif-

 ©1992 American Vacuum Society

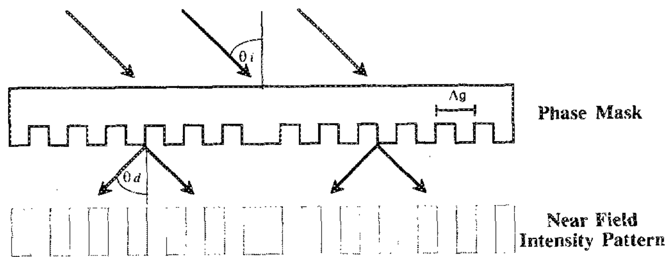

FIG. 1. Schematic diagram of near field printing of grating like pattern by interference of zero-order and first-order diffracted beams.

fracted beam. One can also see from the peak and valley alignments the obvious result that, away from the slightly smeared phase-shift location itself, the phases of the two regions are properly shifted. The important point in Fig. 2 is the gradual broadening of the abrupt phase shift, indicating that the smearing is confined to a few grating periods as long as the gap between the mask and the sample is kept in the range of a few microns. While the Fresnel approximation to the steep-angled propagation after the mask is obviously of limited validity, it does qualitatively suggest that the printing technique can be used to reproduce local grating features when used in the near field.

In the example above only the undiffracted (zeroth order) transmitted beam and the first order diffracted beams are included. For light at wavelength λ incident at an angle θ_i, we have $k_{x_0}=(2\pi/\lambda)\sin\theta_i$. The grating at pitch Λ_g produces diffracted orders m with the k_x values $k_{x_m}=k_{x_0}+m2\pi/\Lambda_g$. For the grating pitches studied here in the range of $\Lambda_g\sim 240$ nm, and illumination at a wavelength of $\lambda\sim 364$ nm, we find that indeed only the $m=0$ and $m=-1$ orders satisfy $|k_{x_m}|<2\pi/\lambda$ as required for non-evanescent propagation after the mask. In fact, to generate *any* diffracted wave that propagates after the mask requires that $\sin\theta_i>\lambda/\Lambda_g-1$, or $\theta_i>31°$.

This article reports on the methods used to fabricate the first-order phase-grating masks intended for use in near-field holographic printing. We also characterize the impact of grating parameters on diffraction efficiency and present our preliminary results using these masks to print gratings.

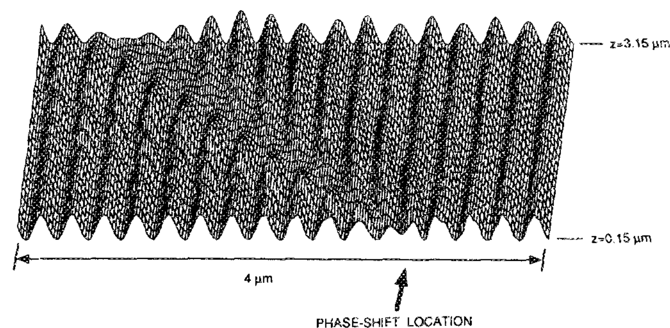

FIG. 2. Spatial evolution of near-field intensity modulation using a phase-grating mask with an abrupt shift in the grating near the arrow.

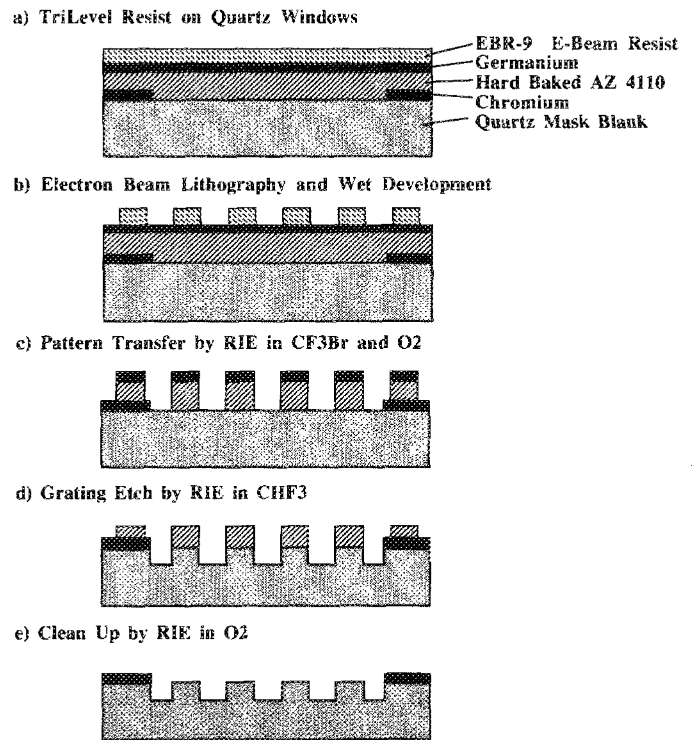

FIG. 3. Schematic diagram of the steps used to fabricate the phase grating in fused silica in the windows opened in the chromium coating.

II. PHASE-GRATING MASK FABRICATION

We have adopted a two level e-beam process to produce the actual square-wave phase masks. Our starting substrate is a chromium coated fused silica photomask blank. In the first step, we define the regions of the blank in which the chromium is to be opened by wet-chemical etching. In this example the mask is designed to print gratings for DFB lasers. The first level therefore includes: windows for gratings at each device site; fiducial mark which indicate cleave positions; alignment marks; and windows for etch depth monitors. These features are quite coarse and can readily be patterned using conventional photolithography. EBL in PMMA was used for expediency in the initial tests. The second lithography level is a high-resolution step in which the square-wave grating is formed in the windows previously opened in the chromium level as well as large squares used as etch depth monitors. Ironically, since the high-resolution step requires a small diameter e-beam, a resist with lower dose requirements was needed. This requires some compromise between throughput and resolution in the imaging layer. EBR-9 (Ref. 4) was therefore used to shorten the overall writing time. The gratings for this work were contained within a single writing field in order to avoid field stitching errors within the area spanned by individual devices.

The details of the second level process is shown schematically in Fig. 3. Both single layer and trilayer schemes were tried as masking layers for the RIE etch mask. The figure illustrates the trilayer resist scheme which was judged necessary to produce square-wave profiles. The

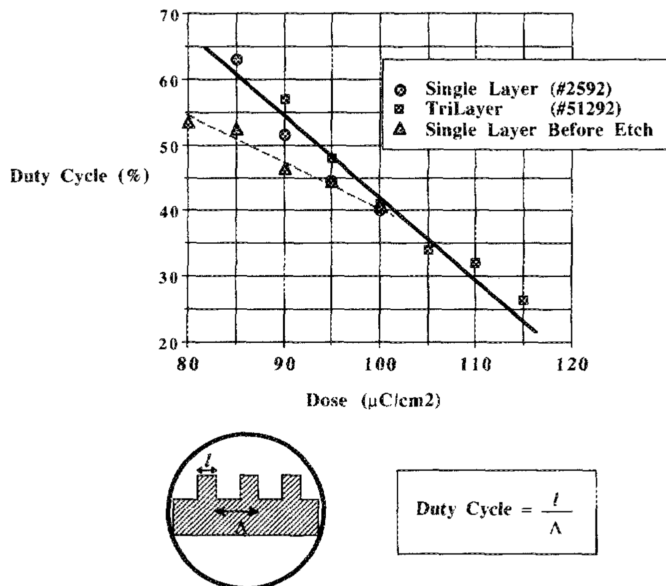

FIG. 4. The relationship between e-beam dose in the resist and the resulting grating duty cycle (defined in the inset) in the phase mask for: single layer EBR-9 (circles) and trilayer (squares). Also shown is the duty which was measured in the resist prior to etching for the single layer resist case.

grating pattern is written in the opened windows but overlapped a small amount with the chromium at the edge. After development in 4:1 methyl isobutyl ketone: isopropanol the pattern is transferred into the thin Ge and hardbaked photoresist by RIE using CF_3Br and O_2, respectively. The resulting pattern is etched into the fused silica using RIE in CHF_3. The etch mask is then removed in an oxygen RIE. Generally, linewidths are not preserved during the process, especially since the CHF_3 etch step can deposit polymer on the sidewalls of the etch mask while removing material from the bottom of the grooves in the fused silica. Figure 4 shows the duty cycle variation with e-beam dose for the resulting gratings, prepared using both single layer EBR-9 and the trilayer. For comparison, the duty cycle of the imaging layer is plotted for the trilayer sample prior to pattern transfer. We note that the single layer and trilayer both appear to have similar dependence but there can be a significant difference between the initial pattern and the resulting groove width.

The typical grating periods for this work ranged from 225 to 240 nm and were 15 μm long in the groove direction and about 400 μm wide, therefore comprising about 1600 periods. This represents the approximate area of a single laser. This pattern was repeated 512 times on the prototype mask (although many more sites are available on the mask). We have written as many a 8 different grating periods in this same range on a single mask.

III. PHASE-MASK CHARACTERIZATION

The period of the gratings were determined by precisely measuring the first-order diffraction angle. The sample is mounted on a rotation stage and illuminated with an argon ion laser ($\lambda = 363.8$ nm). The beam incident on the grating

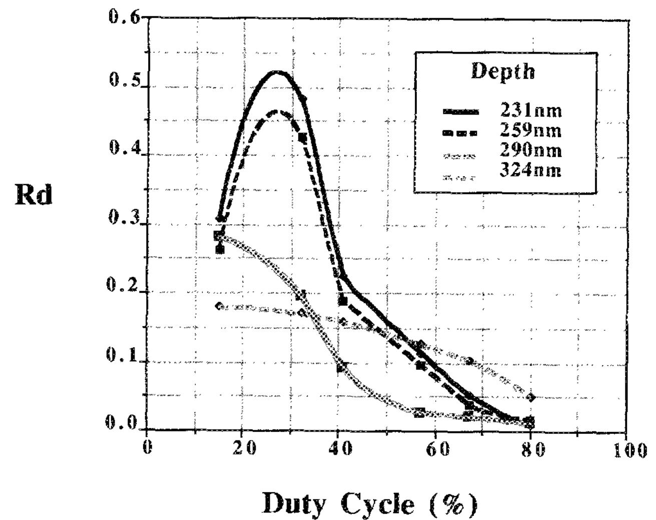

FIG. 5. Measured ratio of the first-order diffracted power to the transmitted power as a function of duty cycle for various etch depths for the single layer resist case.

results in a specularly reflected beam, a transmitted beam, a forward diffracted beam, and a backward diffracted beam. The sample is first oriented to specularly retroreflect the incident beam. The sample is then rotated to align the backwards first-order diffracted beam to retroreflect upon the incident beam path. The difference in angle between these two positions (49.28° for the $\Lambda = 240$ nm gratings) determines the period of the grating by simple geometry

$$\Lambda_g = \frac{\lambda}{2 \sin \theta}.$$

Gratings fabricated in ten different test lots yielded a mean deviation from the design period of 0.05%. Since our simple angular measurement was limited to a resolution of 2 min of arc, this value appears measurement-limited.

Using a similar experimental arrangement, we have measured the power in the transmitted and forward diffracted beams. A lens is inserted between the incident TE-polarized beam and the mask in order to focus the entire laser beam within the grating area. The power into the zero- and first-order diffracted beams are sequentially measured using a detector large enough to fully capture each beam. The highest contrast in the image is obtained when the power into the zero- and first-order beams are equal. If we define C as the ratio of the intensities at the maxima and minima, and R_d as the ratio of the first-order diffracted power to that of the transmitted power, then

$$C = \left(\frac{\sqrt{R_d} + 1}{\sqrt{R_d} - 1} \right)^2.$$

Since $R_d = 1$ is the desired optimum, we sought to determine the effects of grating duty cycle and etch depth on this power ratio. Initial results were obtained for gratings fabricated using the single layer resist process described above. Figure 5 is a plot of four different etch depths. The trends indicate that there is a peak in the beam ratio for duty cycles near 30%. We also note that for all depths the

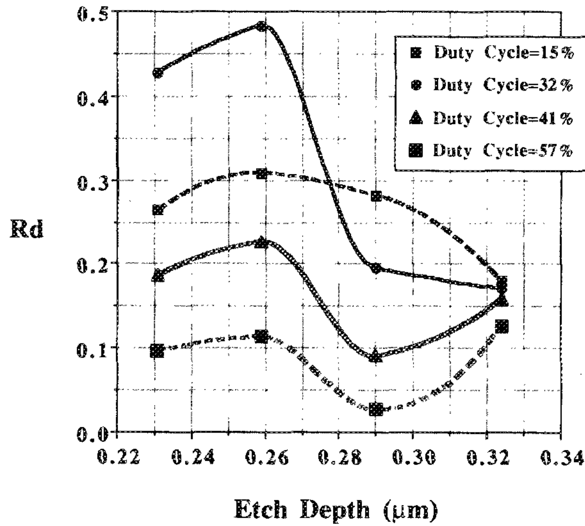

FIG. 6. Measured ratio of the first-order diffracted power to the transmitted power as a function of etch depth for various duty cycles for the single layer resist case.

diffracted beam is weak, peaking at about half the transmitted power. Figure 6 replots the data to illustrate the dependence of the power ratios on etch depth. There appears to again be a peak rather than the expected continuous increase in the diffracted power with deeper etching. Some of this behavior can likely be attributed to nonideal groove profiles. Subsequent fabrication included the trilayer resist process shown in Fig. 3. This scheme is expected to produce improved square-wave gratings with steeper sidewalls. This is supported by the improved diffraction efficiency of the resulting gratings. Figure 7 shows our most recent data for R_d dependence on duty cycle for the trilayer processed gratings. We observe that the values of R_d bracket the balanced beam condition (i.e., $R_d=1$). This is also achieved at a substantially shallower etch depth than needed in the single layer case.

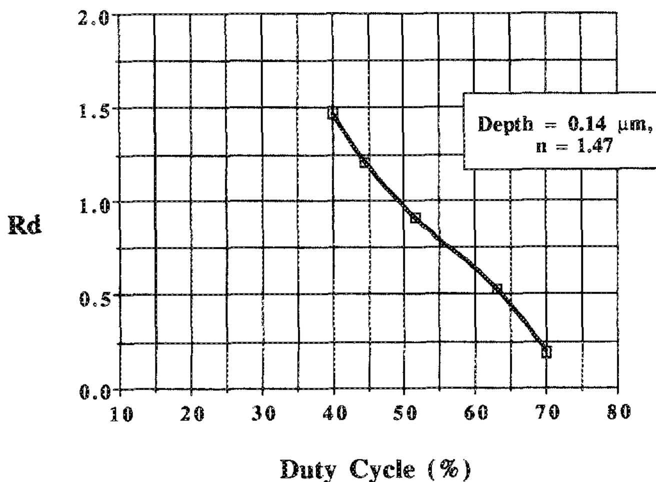

FIG. 7. Measured ratio of the first-order diffracted power to the transmitted power as a function of duty cycle for various etch depths for the trilayer resist case.

IV. THEORY

To predict the effects of the various physical parameters on the diffractive properties an analytical model would be desirable. The simple approach using scalar diffraction theory would proceed as follows. The field just after the mask is assumed to be the incident field multiplied *locally* by a spatially varying phase retardation. This "phase plate" is evaluated simply by propagating the incident field in each region ignoring diffractive effects during the propagation through the mask itself. Thus the empty regions of the square wave suffer a phase retardation

$$\phi_1=k_{z_{\rm air}}d=(2\pi/\lambda)d\cos\theta_i,$$

where d is the tooth height. The regions in the teeth of the grating suffer a phase retardation

$$\phi_2=k_z'd=(2\pi n/\lambda)d\cos\theta',$$

where n is the material index and θ' is the refracted angle, with

$$n\cos\theta'=(n^2-\sin^2\theta_i)^{1/2}$$

from Snell's law. The relative phase delay is then $\phi_d\equiv\phi_2-\phi_1$. Up to a constant phase factor, in the plane just after the grating defined as $z=0$, the field is thus assumed to have the form

$$E(x)=\exp\left(\frac{2\pi}{\lambda}x\sin\theta_i\right)F(x),$$

where

$$F(x)=\begin{cases}1 & \text{for } |x-(2J+1)\Lambda/2|<(1-f)\Lambda/2\\ \exp(i\phi_d) & \text{for } |x-J\Lambda|<f\Lambda/2\end{cases}.$$

Here $J=0, \pm 1, \pm 2, \ldots$, and $f\in(0,1)$ is the grating duty cycle defined as the fraction of the grating period composed of the grating material of index n. As indicated above,

$$\phi_d\equiv\frac{2\pi}{\lambda}d[(n^2-\sin^2\theta_i)^{1/2}-\cos\theta_i].$$

The expression for the field is Fourier decomposed to

$$E(x)=\exp\left(\frac{2\pi}{\lambda}x\sin\theta_i\right)\sum_{m=-\infty}^{\infty}a_m\exp\left(i\frac{2\pi m}{\Lambda}x\right),$$

where

$$a_m=\frac{1}{\Lambda}\int_0^\Lambda F(x)\exp\left(-i\frac{2\pi m}{\Lambda}x\right)dx.$$

These expressions from the simple scalar diffraction theory lead to the conclusion that the zeroth order (undiffracted) and the mth diffracted beams have the fractional powers

$$|a_0|^2=1-4f(1-f)\sin^2(\phi_d/2)$$

and

$$|a_m|^2=\frac{4\sin^2(m\pi f)}{m^2\pi^2}\sin^2(\phi_d/2).$$

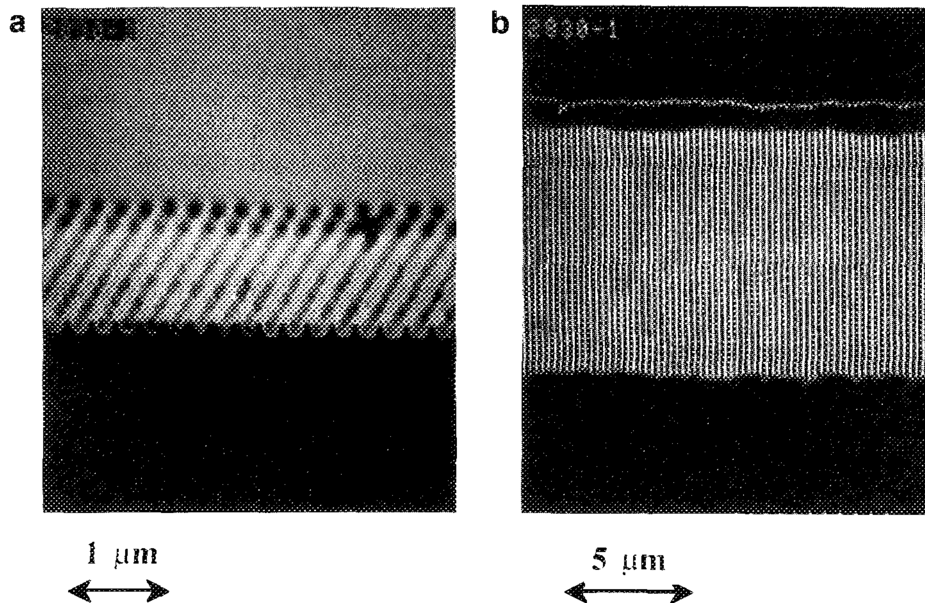

FIG. 8. SEM of gratings etched in InP by RIE using resist mask patterned with near-field holography illuminated with argon laser.

For a 50% duty cycle ($f=1/2$), it is easily seen that the first diffracted and the undiffracted beam have equal intensities at $\phi_d=2\tan^{-1}(\pi/2)$. For an index of $n=1.5$ and a wavelength of $\lambda=363.8$ nm, equal intensity for an incident angle of 49.28° is predicted for a groove depth of $d=181$ nm. This theory also suggests that the most power that can be diffracted into the first order is 40.5%. The simple scalar diffraction theory results in R_d given by

$$R_d=\frac{4\sin^2(\pi f)\sin^2(\phi_d/2)}{\pi^2[1-4f(1-f)\sin^2(\phi_d/2)]}.$$

This rises through the $R_d=1$ condition to infinity when the undiffracted wave intensity has a zero.

An obvious flaw of the treatment given above is that this also predicts an equal power diffracted into the $m=+1$ order, which as we saw earlier was not even a propagating wave. The simple scalar diffraction theory predicts power diffracted into other higher orders which are also evanescent. Also, there is no polarization dependence to the theory. The flaw here was the crude assumption that the field after the mask is simply the incident field multiplied by a phase retardation locally evaluated with ray optics. Since this ignores diffractive effects going through the mask, it is woefully inadequate when the grating features become comparable to the incident wavelength. In the case here, each grating tooth is only a third of the optical wavelength, and a more rigorous diffraction theory is required.

Diffraction from phase gratings of arbitrary pitch and profile has been formulated in a rigorous manner by Moharam and Gaylord.[5] The treatment makes full use of the Maxwell equations including proper treatment of boundary conditions and reflected waves. While it requires numerical evaluation, it can easily yield high accuracy without excessive computation time. While the general cyclic behavior of the diffracted intensity and undiffracted intensity is qualitatively similar to the scalar theory, the rigorous treatments show that nearly 100% of the power can be diffracted into the first order for a proper depth. Also, the rigorous theories properly indicate that indeed the only waves leaving the sample are the specular and first-order diffracted reflections, and the undiffracted and first-order diffracted transmitted beams. A rigorous treatment of the geometries investigated here is unfortunately beyond the scope of this article and will be the subject of a future article.

Given the flawed qualitative behavior of the scalar theory, it appears a coincidence that it is even close to predicting an optimum depth. We find that the experimentally determined dependence of R_d on etch depth for the structures we have fabricated exhibits more structure than predicted by the theories, appearing to peak near the optimum depth rather than continuing to rise (see Fig. 6). The experimental data showing the dependence of R_d on duty cycle from the single layer and trilayer prepared samples show that the trilayer mask produced a significantly stronger diffracted beam which allowed the beam ratio to approach 1. This may be the result of improved, more ideal groove profiles. A mask produced with the best balanced of the measured values should result in an intensity ratio (C) of 440 between the maxima and minima of the near field image, more than adequate for high-quality printing.

V. IMAGING RESULTS

The printing results shown in Figs. 8 and 9 were made using the same grating mask which had a measured R_d of 0.3, which should produce an intensity ratio near 10. Different illumination sources were used for comparison, since a calculation of the required coherence and collimation revealed that it should be possible to use a simple UV lamp

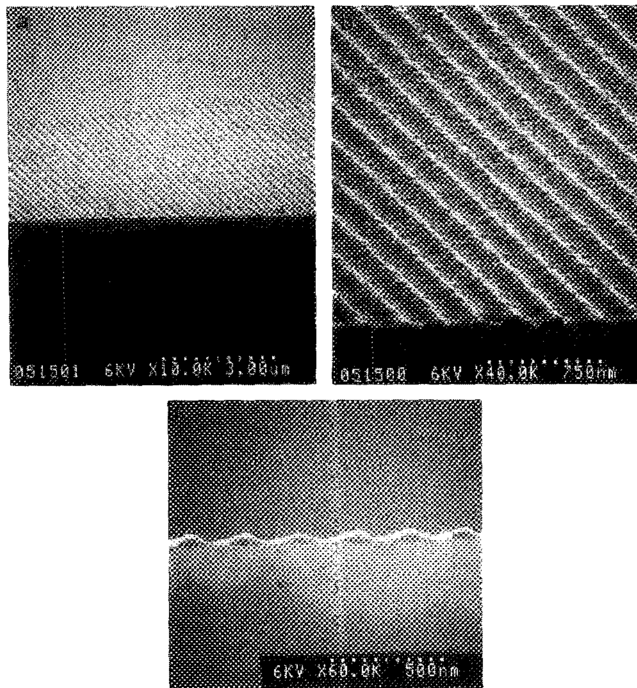

FIG. 9. SEM of developed resist gratings patterned with same mask as the previous figure but illuminated with mercury lamp.

for a gap of up to 10 μm. As described above a gap smaller than this is needed for general printing in this mode, therefore the source should not limit the quality.

Figure 8 shows a scanning electron micrograph (SEM) of a grating which was first printed using Ar laser illumination in 44 nm thick Shipley S1400-3 resist. The developed resist pattern served as a RIE mask in a methane/hydrogen etch of the InP wafer to a depth of 120 nm. A cleaved portion of the 240 nm period etched InP grating is shown in the micrograph. A second exposure was made using the triplet at 365 nm from a mercury/xenon lamp. A small source sized 100 W lamp was chosen to allow collimation with only a condenser lens. The SEM in Fig. 9 shows the developed resist which has been coated with a thin layer of AuPd for inspection. The exposure time was 5 s in 50 nm of AZ 1350J resist. The printed grating is quite good and is uniform over a large area.

VI. CONCLUSIONS

Near-field holographic printing appears to be a powerful and viable method of printing gratinglike structures. It combines the flexibility of direct write EBL with the throughput of UV contact photolithography. Pitch control in our initial trials appears to be at least 0.1 nm for periods near 0.24 μm, presently limited by our ability to measure the diffracted angle. Both duty cycle and the groove depth in the fused silica phase masks were found to be important parameters for obtaining nearly balanced diffracted and undiffracted beams; the condition desired for maximum printing contrast. To model the optimum parameters for the square-wave phase masks, we discussed the grating behavior using a simple scalar diffraction theory. While the general behavior of the diffraction is informative, this simple view is inadequate to provide quantitative predictions. A more rigorous approach has been treated in the literature and a limited comparison indicates much improved agreement with the our data. Our best sample to date was produced using a trilayer resist scheme. It has diffraction ratios as high as 1.5 depending on duty cycle.

Printing tests with a nonoptimized mask appears quite promising. Similar gratings were produced using both highly coherent laser illumination and as well as incoherent illumination from the 365 nm triplet of a mercury lamp. Although further refinement is needed, this method has the potential of replacing the interfering laser beam technique as the method of choice for printing the structures needed for optoelectronic integration.

ACKNOWLEDGMENTS

The authors wish to thank R. Tiberio of the NNF at Cornell University for helpful suggestions for fine pitch adjustment of the gratings, Y. Kosaka and Y. Nakagawa at JEOL USA for helpful suggestions to extend the range of the grating period adjustment. The authors also wish to thank J. Pastalan for his technical assistance in preparing gratings to test the fine pitch control. The authors thank T. R. Hayes, C. A. Green, and R. Pawelek for the processing the grating on InP presented in Fig. 8. Finally, the authors wish to thank M. G. Moharam and J. G. Leger for helpful discussions on diffraction from the phase gratings.

[1]M. Okai, S. Tsuji, N. Chinone, and T. Harada, Appl. Phys. Lett. **55**, 415 (1989).
[2]R. C. Tiberio, G. A. Porkolab, M. J. Rooks, E. D. Wolf, R. J. Lang, A. Larsson, S. Forouhar, J. Cody, G. W. Wicks, T. Erdogan, O. King, and D. G. Hall, J. Vac. Sci. Technol. B **9**, 2842 (1991).
[3]C. E. Zah, C. Caneau, S. G. Menocal, A. S. Godz, P. S. D. Lin, F. Favire, A. Yi-Yan, T. P. Lee, A. G. Joyner, and C. H. Joyner, Electron. Lett. **25**, 650 (1989).
[4]A product of Toray Industries, Osaka 530, Japan.
[5]M. G. Moharam and T. K. Gaylord, J. Opt. Soc. Am. **72**, 1385 (1982).